HiSST: 3rd International Conference on
High-Speed Vehicle Science Technology
14 -19 April 2024, Busan, Korea

Convective Heat Flux Analysis for a Scramjet Engine

Ana Maria P. Lara[1], Israel S. Rêgo[2], Lucas A. G. Ribeiro[3], Lucas Galembeck[4], Dermeval Carinhana Jr.[5] and Tiago C. Rolim[6]
Instituto de Estudos Avançados, São José dos Campos, São Paulo, 12228-001, Brasil

Abstract

The scramjet engine is a hypersonic airbreathing propulsion system based on supersonic combustion. This work investigates the heat fluxes expected in one such engine using analytical approaches. The engine model consists of an inlet composed by a blunt leading-edge region and three compression ramps (compression section), by the combustion and expansion sections. The model is designed to operate at hypersonic speeds in the stratosphere, so it is subjected to high heat transfer loads, specifically on the leading edge. Fay and Riddell's theory, Lees' theory, and Eckert's theory are applied to study the aerodynamic heating at the stagnation point, blunt region, and flat regions of the engine model, respectively. Four models are considered for the determination of the thermodynamic properties and for the calculation of the heat flux, being: calorically perfect gas with and without boundary layer effects, and thermodynamic equilibrium gas with and without boundary layer effects. The highest values of heat flux were found at the stagnation point, followed by a reduction of 96% immediately downstream of the blunt nose. The greatest increases in the heat flux in the flat regions were due the transition from laminar to turbulent flow regimes, and due to the passage of the flow through the reflected shock wave at the isolator entrance. The lowest heat flux values were found in the flat regions while the flow was still laminar, from the start of the first compression ramp to halfway through the second compression ramp.

Keywords: *hypersonic, scramjet, heat flux.*

Nomenclature

Latin

c_p – Specific heat at constant pressure
H – Enthalpy
L – Lewis number
M – Mach number
p – Pressure
Pr – Prandtl number
R – Radius of the blunt region
r – Recovery factor
S_t – Stanton number
T – Temperature
T_r – Recovery temperature
T_w – Outer wall surface temperature
u – Flow speed

Greek

β – Oblique shock wave angle
γ – Ratio between specific heats
θ – Angle deflection

[1] *Division of Aerothermodynamics and Hypersonics, Institute for Advanced Studies, anamariapereiralara@gmail.com*
[2] *Division of Aerothermodynamics and Hypersonics, Institute for Advanced Studies, israelisr@fab.mil.br*
[3] *Division of Aerothermodynamics and Hypersonics, Institute for Advanced Studies, lucaslagr@fab.mil.br*
[4] *Division of Aerothermodynamics and Hypersonics, Institute for Advanced Studies, galembecklg@fab.mil.br*
[5] *Division of Aerothermodynamics and Hypersonics, Institute for Advanced Studies, dermevaldcj@fab.mil.br*
[6] *Division of Aerothermodynamics and Hypersonics, Institute for Advanced Studies, tiagotcr@fab.mil.br*

θ_1 – Angle of the first ramp
μ – Dynamic viscosity
ρ – Specific mass

Subscripts
e – indicates the properties at the edge of the boundary layer
s – Indicates the properties at the stagnation point
w – Indicates the properties of the wall surface
∞ – Indicates the properties of the freestream

Superscripts
* – Indicates the properties that use the Eckert Reference temperature

1. Introduction

The engine model refers to an academic scramjet design optimized for hypersonic speeds. This model consists of an inlet composed by a blunt leading-edge region and three compression ramps (compression section), an isolator and an internal expansion ramp (combustion section), and an external expansion ramp (expansion section), as illustrated in Fig. 1.

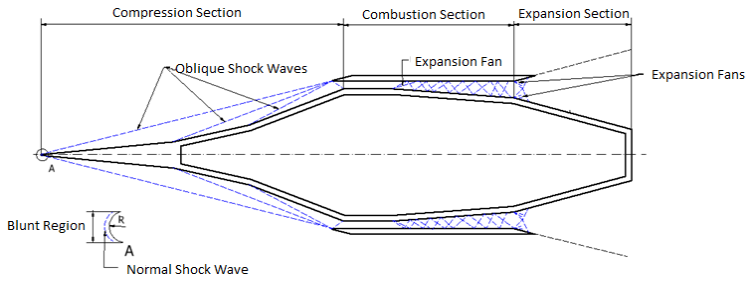

Fig 1. Compression, combustion and expansion section of the academic scramjet model.

In the blunt region of the engine model's leading edge there is the incidence of a normal shock wave that decelerates the flow. Then, the flow is decelerated isentropically to the stagnation point before reaccelerating along the blunt region. In the compression ramps there are the formation of oblique shock waves which compress and decelerate the flow. After combustion, its products are accelerated in the expansion ramps, generating the necessary thrust for the operation of the scramjet.

The shock waves play an important role guiding the flow into the combustion section. Consequently, the engine model uses the physical phenomena occurring during flight to get into operation, as it extracts the necessary oxygen for combustion from the air instead of carrying it on board. The oxygen corresponds about 65% of the total weight fraction of the rockets, and therefore using the scramjet technology there is a large increase in the payload fraction [1].

As the flow convects downstream along the surface of the compression ramps, it naturally transitions from a laminar to a turbulent regime, leading to an increase in pressure and temperature. These changes in thermodynamic properties intensify the heat flux. Given that scramjets operate at hypersonic speeds, aerospace vehicles using this technology are highly susceptible to overheating. Therefore, it is important to perform a comprehensive heat flux analysis in any scramjet design. In recent years, several hypersonic experiments have been conducted. For example, SHEFEX I was intended to analyze the behavior of a new concept of thermal protection during flight [2].

The progress of hypersonic vehicles demands computer simulations, as well as the execution of flight and ground tests. As a consequence of technological advances and software implementation, computer simulations are the starting point for R&D, saving time and resources [3]. This paper studies the heat flux at the stagnation point, the blunt region, and the flat regions of engine model. The analysis considers air as calorically perfect gas both with and without boundary layer effects, as well as thermodynamic equilibrium gas with and without boundary layer effects.

2. Methodology

2.1. Stagnation Point

In the blunt region, a normal shock wave occurs, decelerating the flow to a subsonic speed and resulting an increase in the temperature and pressure. After passing through the normal shock wave, the flow decelerates isentropically up to the stagnation point, leading to further increase in pressure and temperature (Fig. 2).

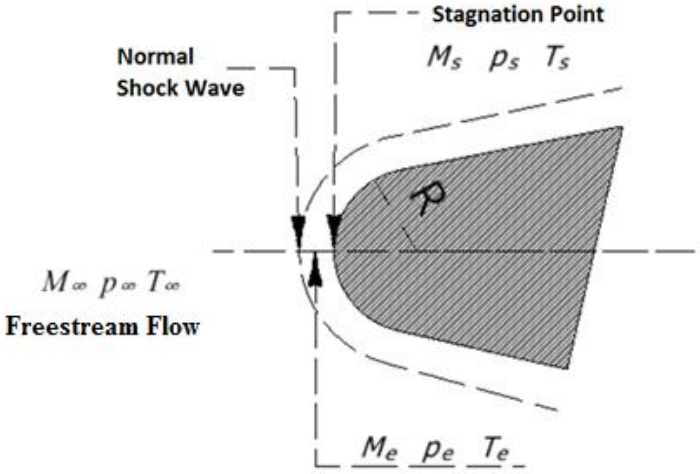

Fig 2. Stagnation point.

The heat flux calculation at the stagnation point (Fig. 2) is performed using a modified version of the Fay and Riddell's theory [4] for cylindrical bodies, as outlined in Ref. [1]:

$$q = 0.57Pr^{-0.6}(\rho_s\mu_s)^{0.4}(\rho_w\mu_w)^{0.1}(h_s - h_w)\left[1 + (L^{0.52} - 1)\frac{h_D}{h_s}\right]\left(\frac{du_e}{dx}\right)_s^{0.5} \quad (1)$$

and the flow speed gradient at the stagnation point $\left(\frac{\mathrm{du}_e}{\mathrm{dx}}\right)_s$ can be obtained by:

$$\left(\frac{\mathrm{du}_e}{\mathrm{dx}}\right)_s = \frac{1}{\mathrm{R}}\sqrt{\frac{2(\mathrm{p_s} - \mathrm{p}_\infty)}{\rho_s}} \quad (2)$$

To calculate the heat flux at the stagnation point, two scenarios are considered: calorically perfect gas and gas in. In the case of equilibrium flows, the thermodynamic state of the gas will be determined by two thermodynamic parameters, such as pressure (p) and temperature (T), or pressure (p) and enthalpy (h). In problems involving equilibrium gas flows, in addition to numerically integrating the gas dynamics equations, it is also necessary to compute the thermodynamic functions for the reactive gas mixture. This is achievable by applying one of several available techniques, such as the Mollier diagram, numerical methods, and by incorporating the equations of statistical thermodynamics into the flow equation.

The boundary layer starts at the stagnation point and its effects are included in the heat flux formulation. The flow properties at the stagnation point, after the normal shock wave are estimated by the relations presented by Anderson [5], which are functions of the properties of the freestream conditions.

Fay and Riddell (1958) assume that the number of Lewis is constant across the boundary layer considering its value varying between 1 and 2. The number of Lewis can to be defined by:

$$L = \frac{\alpha}{D_{AB}} \tag{3}$$

Using the Reynolds Analogy, it can be assumed that the thermal diffusivity and the mass diffusivity are equal, resulting in a Lewis number of 1.

The pressure across the boundary layer, from the surface to its end, is assumed constant, so $p_w = p_s$. Therefore, starting from the equation of state:

$$p = \rho RT \tag{4}$$

the specific mass of the air adjacent to the wall can be calculated by:

$$\frac{\rho_w}{\rho_s} = \frac{T_s}{T_w} \quad \therefore \quad \rho_w = \left(\frac{T_s}{T_w}\right) \times \rho_s \tag{5}$$

Fay and Riddell (1958) consider the wall temperature varying between 300 K and 3,000 K. In this work is assumed an arbitrary value of 300 K and a number of Prandtl of 0.71.

The dynamic viscosity can be determined by the Sutherland equation:

$$\frac{\mu}{\mu_r} = \left(\frac{T}{T_r}\right)^{\frac{3}{2}} \left(\frac{T_r + S}{T + S}\right) \tag{6}$$

where μ_r e T_r are determined as a function of sea level values, given by μ_r= 1.789 x 10^{-5} (N.s/m^2) and T_r= 288K. The constant S is equal to 110 K.

2.2. Blunt Region

The blunt region is represented in the Fig. 3, where the angular variation from the stagnation point to the beginning of the flat regions (first compression ramp) is shown.

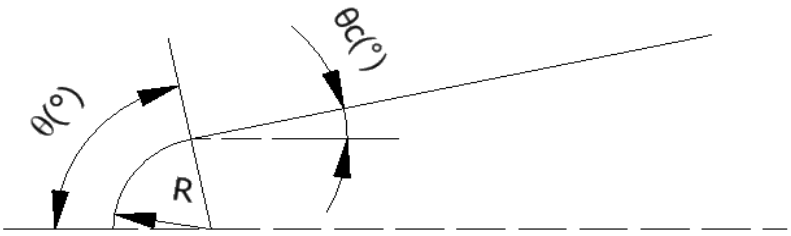

Fig 3. Blunt region.

As done for the stagnation point, two scenarios are considered in calculating the heat flux in the blunt section: calorically perfect gas and thermodynamic equilibrium gas. The heat flux calculation outside the stagnation point of the blunt region is done using the Lees' theory [6], which is dimensioned as a function of the geometric position in relation to the heat flux at the stagnation point. Thus, it is not necessary to know the thermodynamic properties along the blunt region (only the angular variation):

$$\frac{\dot{q}}{\dot{q}_0} = \frac{2\theta \text{sen}\theta\left\{\left[1 - \frac{1}{\gamma M_\infty^2}\right]\cos^2\theta + \frac{1}{\gamma M_\infty^2}\right\}}{[D(\theta)]^{0.5}}, \tag{7}$$

where,

$$D(\theta) = \left[1 - \frac{1}{\gamma M_\infty^2}\right]\left[\theta^2 - \frac{\theta \text{sen}4\theta}{2} + \frac{1 - \cos 4\theta}{8}\right] + \frac{4}{\gamma M_\infty^2}\left[\theta^2 - \theta \text{sen}2\theta + \frac{1 - \cos 2\theta}{2}\right]. \tag{8}$$

2.3. Flat regions

The flat regions comprise three regions of the compression section (1 to 3), three regions in the combustion section (4 to 6), and two regions in the expansion section (7 and 8). In the regions 1, 2, and 3, three oblique shock waves decelerate the flow, and subsequently increase the pressure and temperature (Fig. 4 –A). The inlet is designed so that the oblique shock waves focus on the upper surface of the cowl, generating a reflected shock wave (Fig. 4 – B) before entering the region 4 (part of the combustor). The reflected shock wave causes further deceleration of the flow and increases pressure and temperature.

The flow properties in the regions 1, 2, 3, and 4, following the oblique shock waves, are calculated using the relations presented by Anderson [5], which are dependent on the properties of the local freestream. The angle of the reflected shock wave is the sum of the angles of the three ramps.

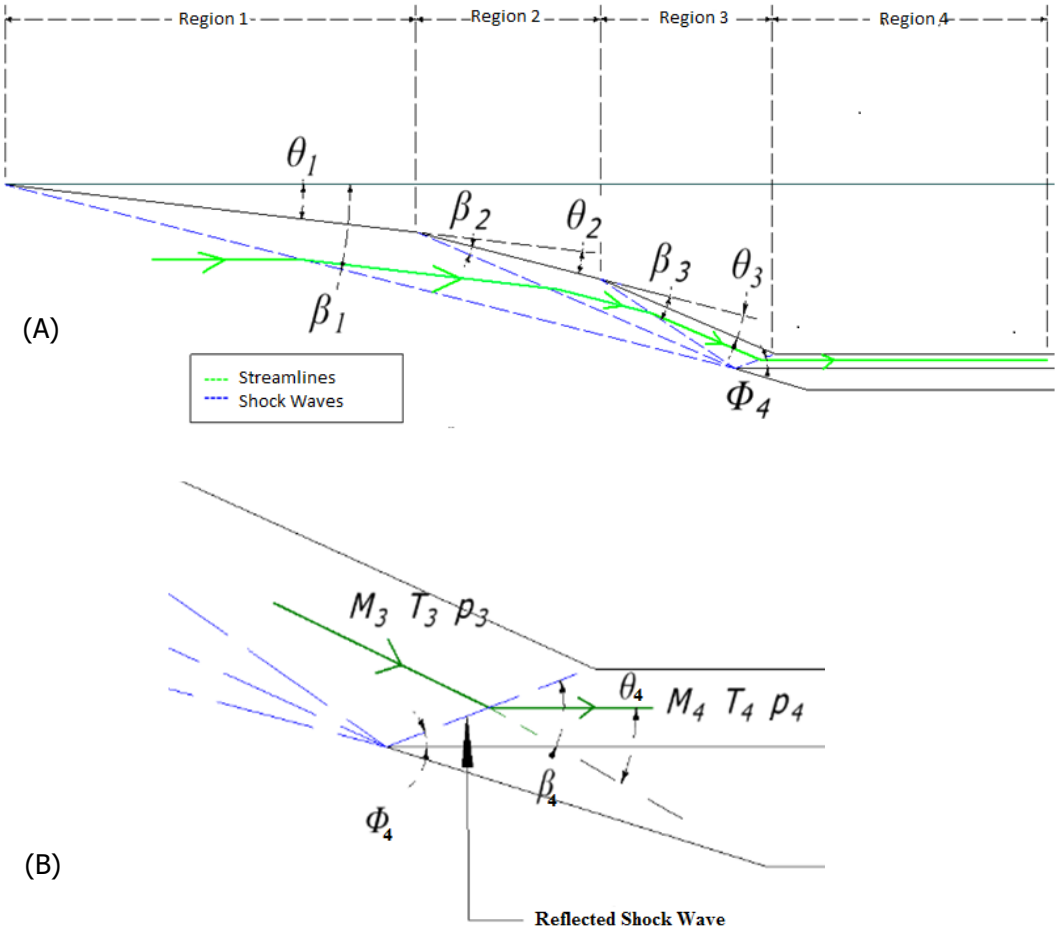

Fig 4. Oblique shock waves (A) and reflected shock wave (B).

In region 5 there is the incidence of an expansion fan, causing the acceleration of the flow and decreasing both pressure and temperature (Fig. 5 - A). It is assumed that the beginning of region 6 occurs after the first reflection of the most upstream Mach wave reaches the body of the scramjet. This distance varies according to the adopted modeling, as it depends on the upstream thermodynamic properties. The Mach waves of the expansion fan continue to reflect along the region 6 (Fig. 5-B). In region 7, two expansion fans induce flow acceleration, resulting in pressure and temperature reduction. Mach waves arising from the two expansion fans undergo further reflections. It is assumed that the region 8 starts after the Mach waves, reflected at the intersection, hit the opposing walls (Figure 5 - C).

The thermodynamic properties in regions 5 and 7 are calculated using the Prandtl-Meyer theory, and in regions 6 and 8 they are determined using the quasi-one-dimensional isentropic flow equation that relates cross sectional area and Mach number [4].

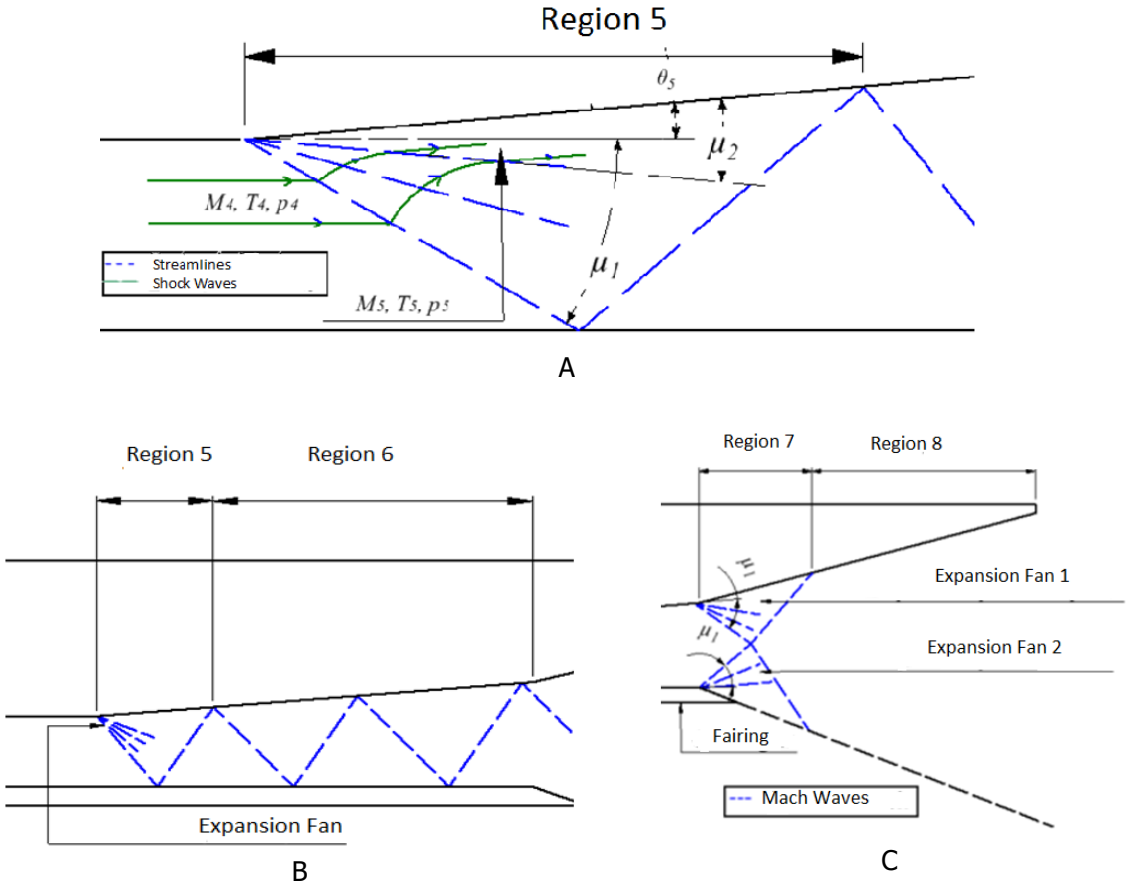

Fig 5. Regions 5, 6, 7, and 8 of the academic scramjet model.

The calculations of the thermodynamic properties considering the effects of the boundary layer are done using the displacement thickness method as in Bonelli et al. [7]:

$$\frac{\delta^*}{x} = \sqrt{\frac{C^*}{Re_{\infty,x}}} \left(1.72 + 2.21 \frac{\gamma - 1}{2} M_\infty^2 + 1.93 \frac{T_w - T_r}{T_\infty} \right) \tag{9}$$

which consists of the following steps: 1) Obtain the thermodynamic properties of the undisturbed local flow; 2) Calculate the thermodynamic properties downstream of the physical phenomena that occurs in each region considering the ramp angle ($\theta_1, \theta_2, \theta_3, \theta_4$); 3) Verify if the flow is laminar, transitional, or turbulent, using the local Reynolds number for hypersonic speed; 4) Calculate the displacement thickness of the boundary layer (δ^*) using Equation 9, and the angles from this thickness (θ_1', θ_2', θ_3', θ_4'). It is considered in this paper that the boundary layer starts at the beginning of the plane section of the scramjet body and continues growing, so the displacement thickness of the boundary layer is summed up in each region ($\sum_{i=1}^{8} \delta_i{}^*$). In the cowl, the properties are considered to be the same as the scramjet body at each time. Consequently, the thickness of the boundary layer is calculated starting from the sharp leading edge of the cowl; 5) Finally, calculate the thermodynamic properties considering the angle from the displacement thickness of the boundary layer (θ_1', θ_2', θ_3', θ_4') and the output properties of the downstream region taking into account the effects of the boundary layer (Fig. 7).

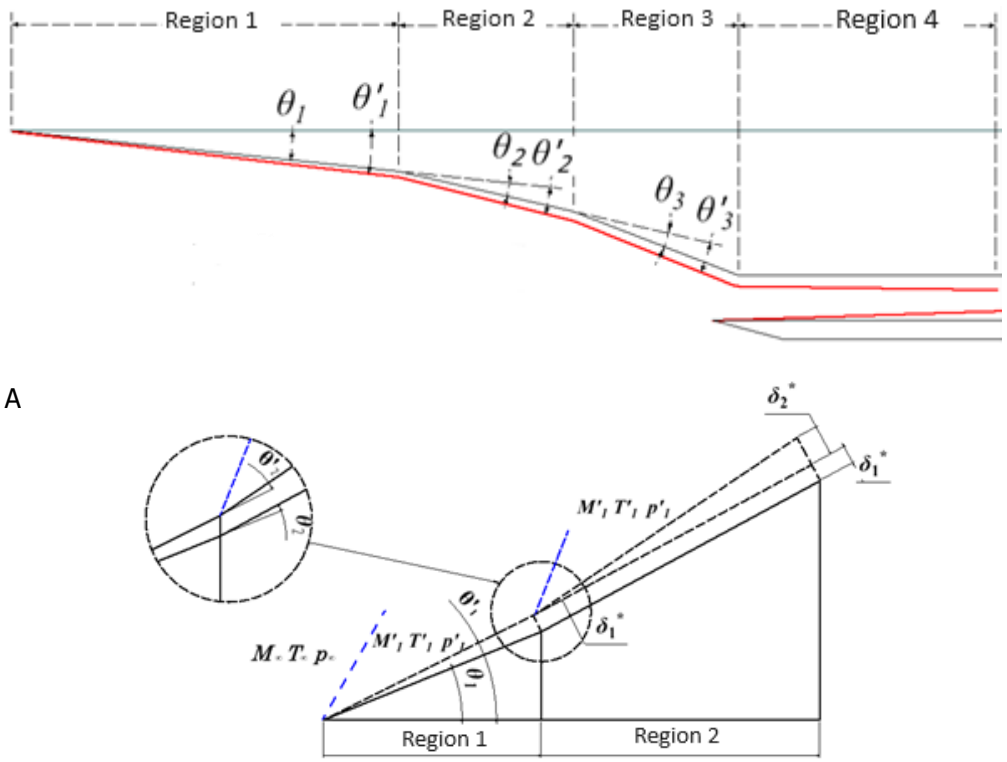

Fig 7. Displacement thickness of the boundary layer along the compression section (A). Methodology for calculating thermodynamic properties considering the boundary layer effects (B).

The calculation of the heat flux in flat regions is done using the theory of Eckert [8]:

$$\dot{q} = S_t^* \rho^* u_e c_p (T_r - T_w). \tag{10}$$

The Stanton number can be used for laminar and turbulent regime, Equations 11 and 12 respectively.

$$S_t^* = \frac{0.332}{P_r^{\frac{2}{3}} (Re_x^*)^{\frac{1}{2}}}, \tag{11}$$

$$S_t^* = \frac{0.0287}{P_r^{\frac{2}{5}} (Re_x^*)^{\frac{1}{5}}}. \tag{12}$$

The Reynolds number Re_x^* is given by:

$$Re_x^* = \frac{\rho^* V_e x}{\mu^*}, \tag{13}$$

and x is used as the characteristic length of the flow.

In order to correct the effect of the high-speed on the variation of properties, all properties with superscript * are calculated by substituting the conventional temperature with the reference temperature of Eckert (T^*), which is given by:

$$T^* = T_e + 0.5\,(T_w - T_e) + 0.22\,(T_r - T_e), \tag{14}$$

where the recovery temperature T_r,also known as adiabatic wall temperature, is given by:

$$T_r = T_e\left[1 + r\frac{\gamma - 1}{2}M_e^2\right], \tag{15}$$

and the recovery factor (r) for laminar flow is: $r = \sqrt{Pr}$, and for turbulent flow, $r = \sqrt[3]{Pr}$.

3. Results and Discussion

The maximum heat flux along the scramjet is observed at the stagnation point, attributed to the reduction of speed to subsonic regime induced by the normal shock wave and the subsequent isentropic deceleration towards the stagnation point. For the calorically perfect case, a heat flux of 4,408 kW/m² was found, while considering the gas in thermodynamic equilibrium resulted in 3,743 kW/m² (about 15% less), (Fig. 8).

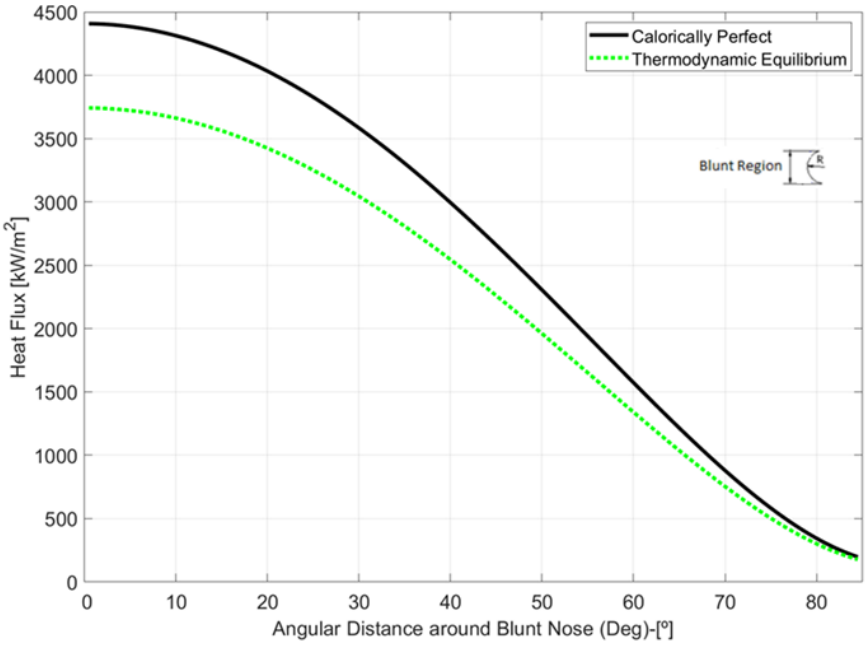

Fig 8. Heat flux along the angular distance around the blunt region of the engine model.

The heat flux decreases sharply along the first compression ramp, dropping by about 64% within the first 20% of the ramp, and reaching approximately 37 kW/m² at the end of the ramp. As can be seen

in Fig. 9, the heat flux curves for the four models are very close, with cases considering boundary layer effects exhibiting a slightly higher heat flux (1.75%).

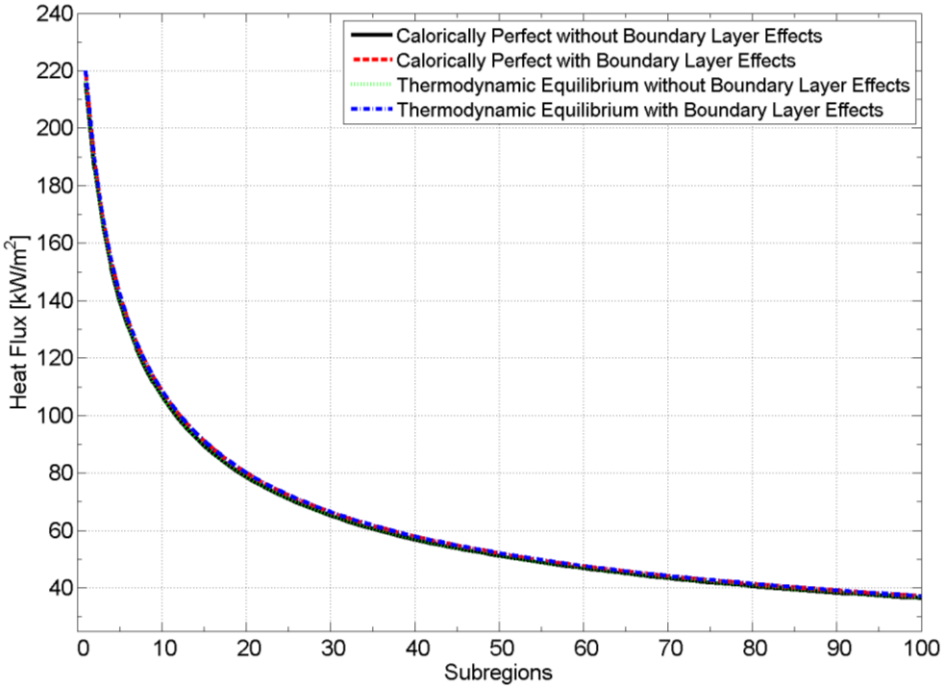

Fig 9. Heat flux along the 1st region.

The passage through the second oblique shock wave causes an increase of almost 60% in the heat flux, resulting in a 21.6 kW/m^2 increase. The heat flux slowly decreases along the first half of the ramp. At that point, the transition from laminar to turbulent occurs, resulting a substantial increase in the heat flux (more than 400%). Then, the heat flux continues to decrease reaching 256 kW/m^2 at the end of the second ramp. As shown in Fig. 10, during the laminar regime, the heat flux remains practically the same regardless of the chosen model. However, after the transition to the turbulent regime, both models with boundary layer effects – calorically perfect and thermodynamic equilibrium – exhibit a slight increase (6%) in comparison with the cases without boundary layer effects.

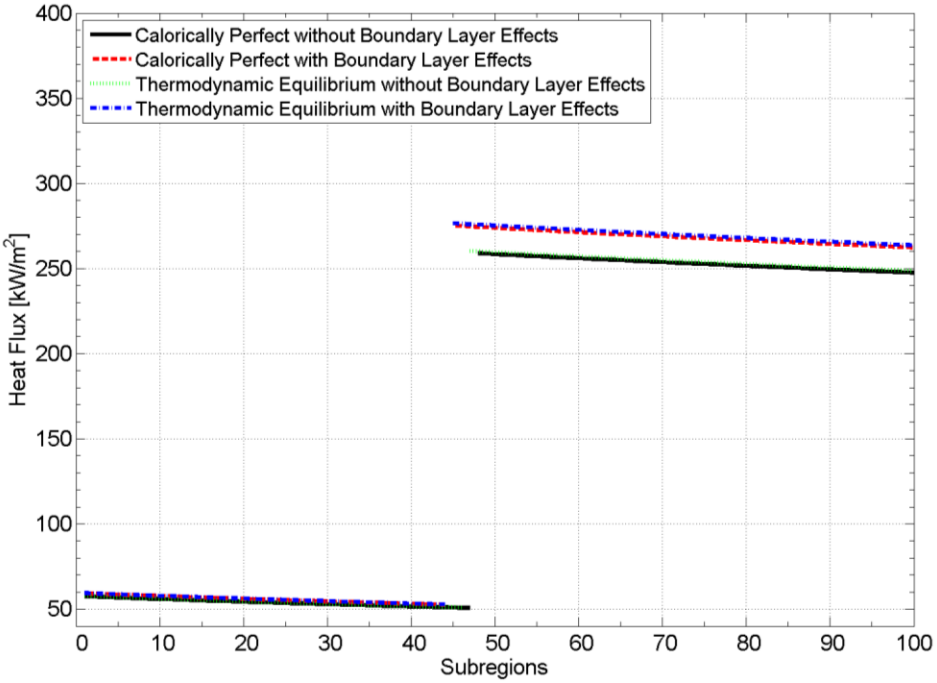

Fig 10. Heat flux along the 2nd region.

Passing through the third shock wave results in a heat flux increase between 250 and 275 kW/m², depending on the model used, followed by a gradual decrease. At the end of the third ramp, the heat flux is about 6% smaller (Fig. 11).

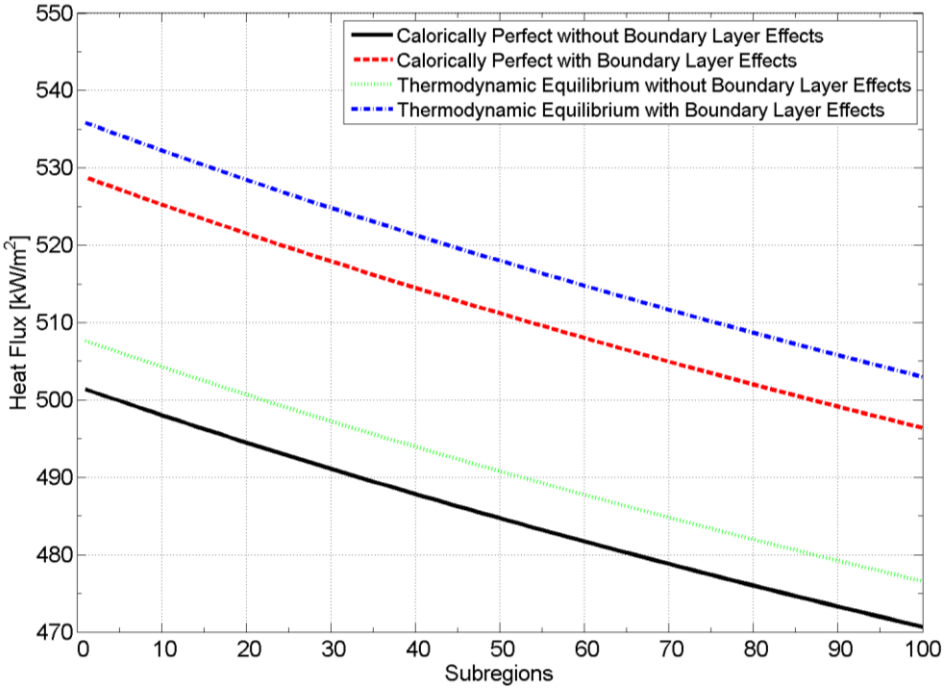

Fig 11. Heat flux along the 3rd region.

The passage through the reflected wave substantially increases the thermodynamic properties of the flow, generating a heat flux increase of about 330%. It gradually decreases along the isolator (4th region), resulting in a heat flux ranging from 1,460 to 1,610 kW/m² at the end of it, depending on the model chosen (Fig. 12).

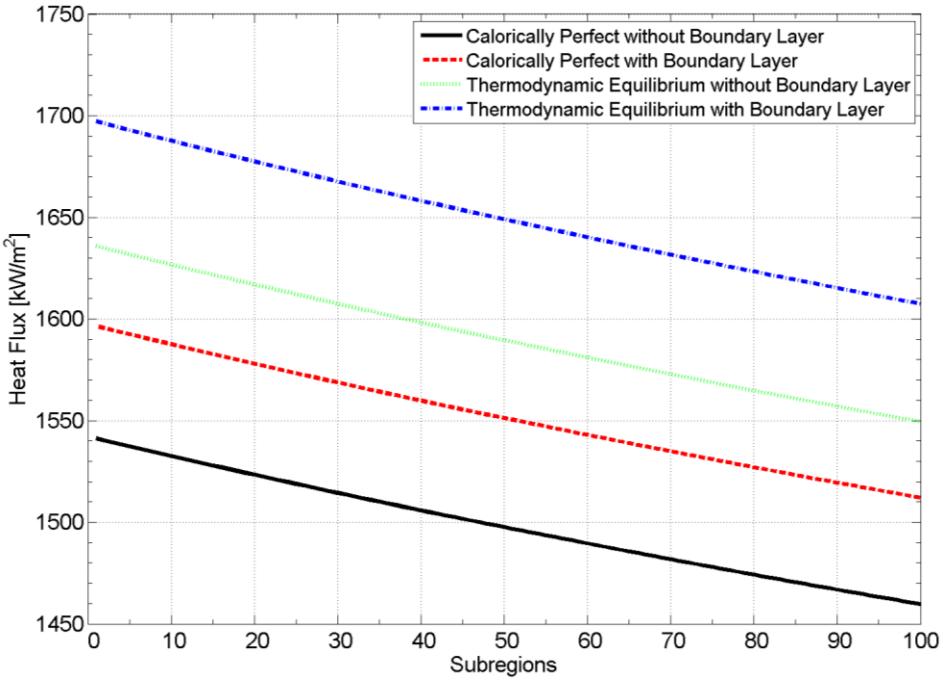

Fig 12. Heat flux along the 4th region.

After the isolator, the flow slightly expands in the 5th region, resulting in a further heat flux decrease of about 2% (Fig. 13).

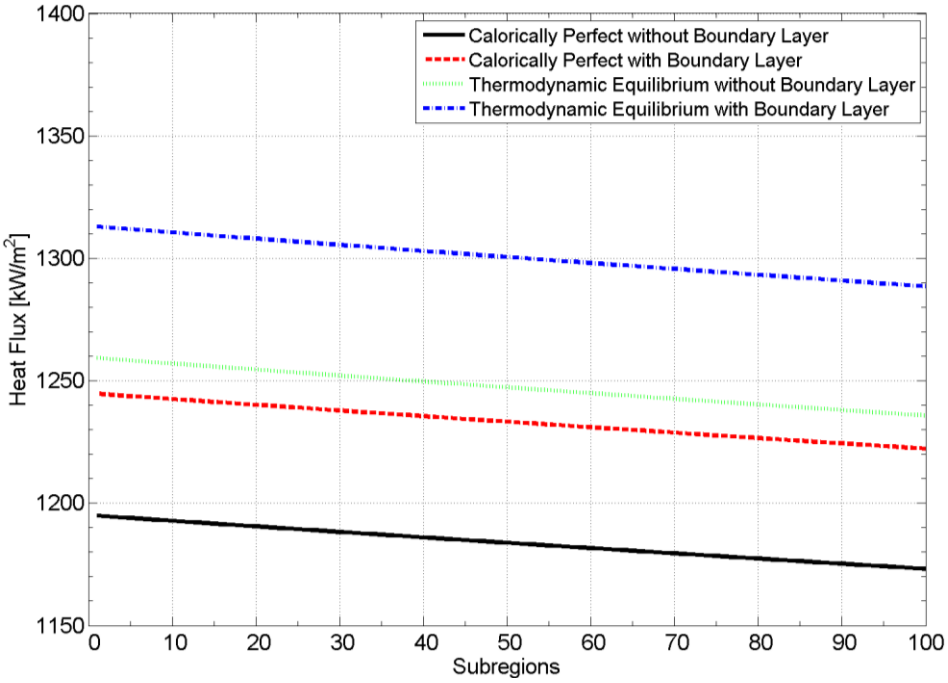

Fig 13. Heat flux along the 5th region.

Moving into the 6th region, which also encompasses an area change inside the combustor, the expansion continues, leading to a substantial heat flux reduction, 41% to 44% depending on the model (Fig. 14).

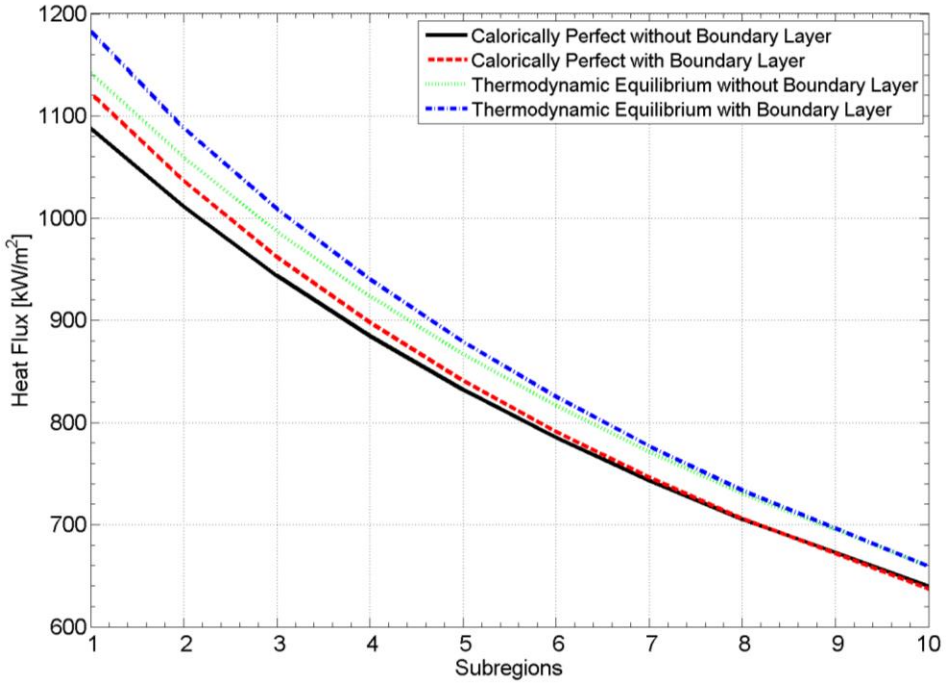

Fig 14. Heat flux along the 6th region.

From the end of the 6th region to the 7th region, a substantial decrease in heat flux occurs, marking the beginning of the expansion section (Fig. 15).

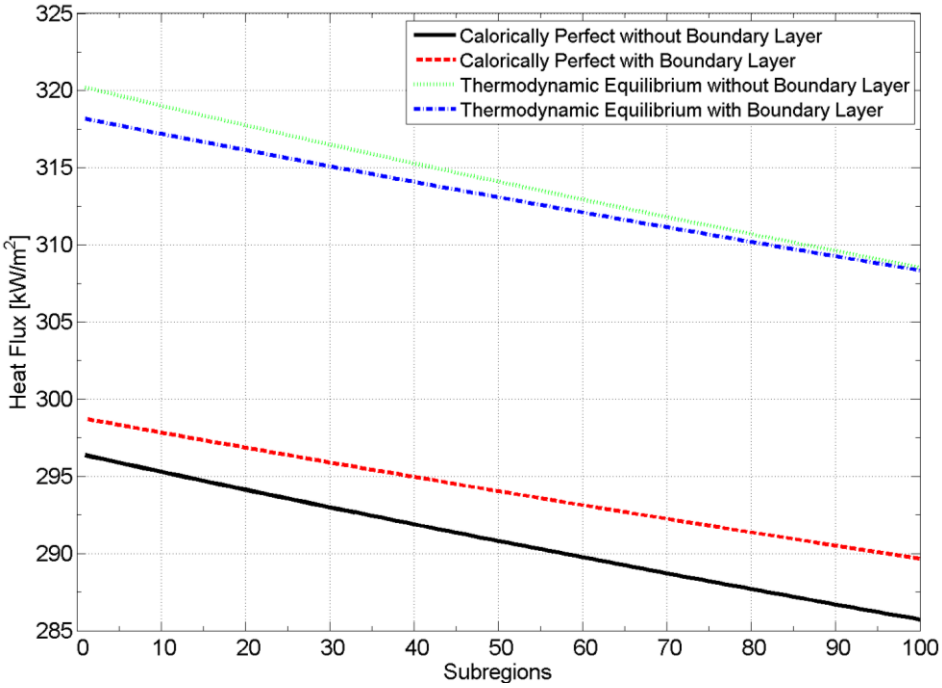

Fig 15. Heat flux along the 7st region.

Continuing into the next region, the 8th, the heat flux continues to decrease, reaching a range from 175 to 220 kW/m² at the end of it, depending on the chosen model (Fig. 16).

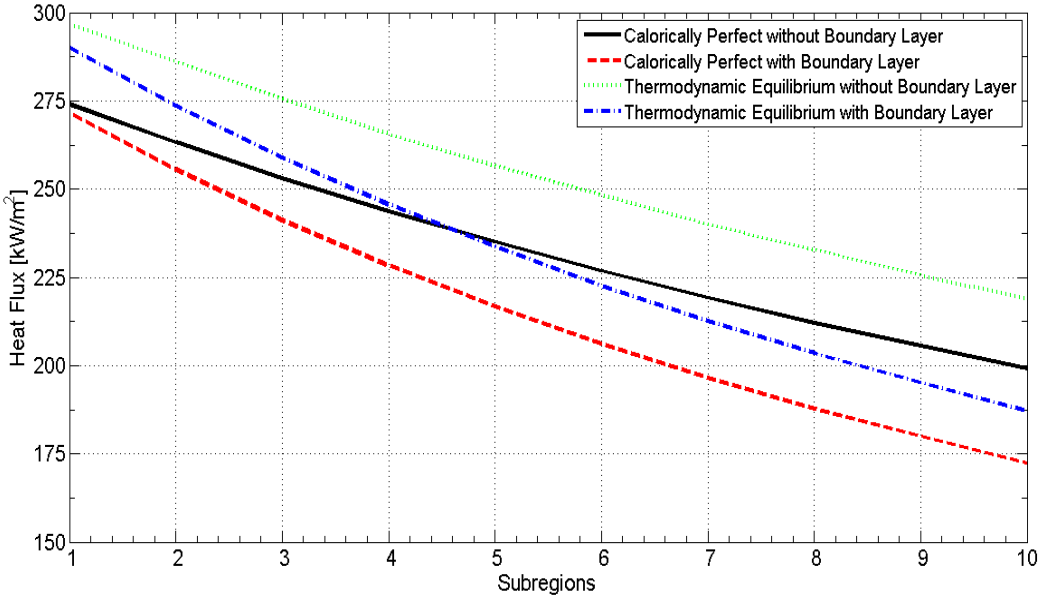

Fig 16. Heat flux along the 8th region.

A summary of the heat flux estimates along the entire academic scramjet model is depicted in Fig. 17 for each of the four models considered: calorically perfect gas with and without boundary layer effects, and thermodynamic equilibrium with and without boundary layer effects. The behavior is quite similar across these scenarios, with slightly more variation observed in the isolator (4th region). Beginning with a substantial decrease in heat flux at the blunt region, this reduction continues gradually along the first ramp. Subsequently, the heat flux increases in the rest of the compression section (regions 2 and 3) and then begins to decrease slowly inside the combustor, intensifying this reduction as the flow undergoes expansion due to the area change. Finally, in the expansion section, as the flow continues to expand, the heat flux consequently continues to decrease.

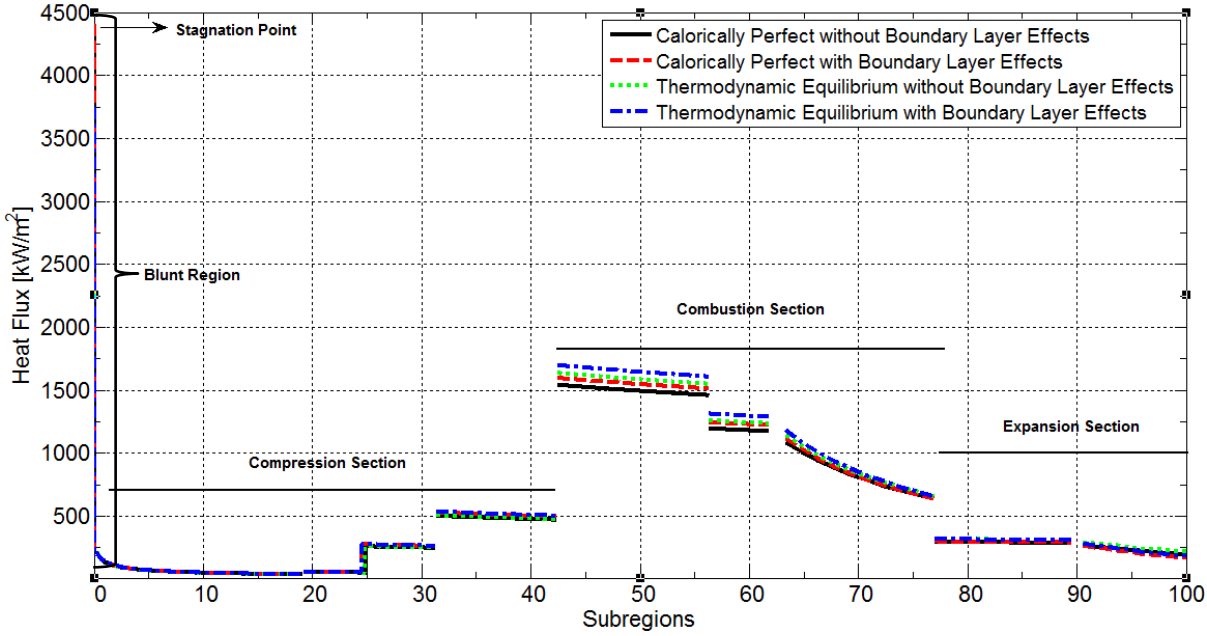

Fig 17. Heat flux along the academic scramjet model.

4. Conclusion

Calculations of the heat flux along at the stagnation point, the blunt region, and the flat regions of an academic scramjet engine model were performed. Four conditions were considered, including calorically perfect gas with and without boundary layers effects, as well as thermodynamic equilibrium gas with and without boundary layers effects. The calculations of the heat flux applied the Fay and Riddell's theory, the Lees´ theory, and the Eckert's theory to study the aerodynamic heating at the stagnation point, blunt region, and flat regions of the engine, respectively. The highest value of heat flux was observed at the stagnation point, followed by a significant reduction of about 96%. Passing through the shock waves increased the heat flux, from approximately 40 kW/m² at the end of the first compression ramp to above 1,500 kW/m² at the combustor entrance. It was also noted that the transition from laminar to turbulent regime increased the heat flux by more than 400%, and the lowest observed heat flux was right before this transition. In the flat regions, the highest heat flux value was observed in the isolator due to the passage through the reflected shock wave. Therefore, these results are important for understanding the heating phenomena in a scramjet model and how they are influenced by the geometry of each section and the physical model applied. Furthermore, future work is suggested to compare the behavioral response with a sharp edge model

Acknowledgements

This work was performed within the 'Technologies for Hypersonic Flights' project, coordinated by the Institute for Advanced Studies, is supported by the Brazilian Funding Agency for Studies and Projects (FINEP) under the Contract no.: 01.22.0255.00 and by the Brazilian Air Force (COMAER).

References

1. Van Driest, E. R. "The Problem of Aerodynamic Heating". *Aeronautical Engineering Review*, pp. 1519-1541, Oct 1956.

2. Souza C.; et al. "Aerodynamic stability analysis for hypersonic experiments." 2nd International Conference on High-Speed Vehicle Science Technology, Bruges, Belgium, 2022.

3. Jefte G.; et al. "Investigation of a Supersonic Combustion Chamber using a Shock Tube". 2nd International Conference on High-Speed Vehicle Science Technology, Bruges, Belgium, 2022.

4. Fay, J. A.; Riddell, F. R. "Theory of Stagnation Point Heat Transfer in Dissociated Air". *Journal of the Aeronautical Sciences*, Vol. 25, pp. 73-85, Feb 1958.

5. Anderson Jr, J. D. "Modern Compressible Flow: With Historical Perspective". New York: McGraw-Hill, 2003.

6. Lees, L. "Laminar Heat Transfer Over Blunt-Nosed Bodies at Hypersonic Flight Speeds". *Journal of Jet Propulsion*, pp. 259-274, April 1956.

7. Bonelli, F.; et al. "Preliminary Design of a Hypersonic Air-breathing Vehicle". *17th AIAA International Space Planes and Hypersonic Systems and Technologies Conference*, p. 14, San Francisco, 2011.

8. Eckert, E. R. G. "Engineering Relations for Heat Transfer and Friction in High Velocity Laminar and Turbulent Boundary-Layer Flow Over Surfaces with Constant Pressure and Temperature". *American Society of Mechanical Engineers.*, pp. 1273-1283, 1955.

9. Heiser, W H. "Hypersonic Airbreathing Propulsion". Washington: AIAA, 1994.